Chapter 6

Multiferroicity and photocatalytic activity in Mg-doped ZnO nanoparticles

6.1. Introduction:

The *n*-type semiconducting nature in ZnO is generally raised from the growth of oxygen vacancies and zinc interstitials in the specimen during preparation. ZnO has an interesting luminescence property that is applicable in optoelectronic and photonic devices, such as UV light emitting diodes (LEDs) and solid state laser diodes (LD's) etc. [15, 16]. The photosensitive properties of ZnO make it a decent photocatalyst to destruct various pollutants [73]. As regard to photocatalytic properties, ZnO is considered to be ahead of other semiconductor photocatalysts due to high redox potential, large exciton binding energy (~60 meV), superior physical and chemical stability and nontoxicity [67, 68]. Yet, pure ZnO has a fast recombination rate of the photo-generated electron-hole pair and thus a low quantum yield in photocatalytic reaction [73]. The low quantum yield puts a limit on its large scale applications on grounds of economic viability. Incorporation of appropriate metal ions in the host ZnO nanoparticles is likely to control the recombination of the photo-generated electron-hole pairs in photocatalysis. Magnesium is one such metallic element considered to decrease the recombination rate in ZnO. The ionic radius of Mg^{2+} (0.66 Å) is slightly less than that of Zn^{2+} (0.74 Å) in a crystal and can be incorporated at the Zn sites of ZnO without producing any lattice strain. The solubility limit of Mg in ZnO is reported to be as high as 20 mol percentage. Further, magnesium is nontoxic and cost effective. Thus Mg doping in ZnO nanoparticles is a suitable approach to achieve better photocatalytic activities.

The band gap of ZnO can be tuned by substitution of dopants like Mg. It is worth pointing here that the band gap of magnesium oxide MgO (7.4 eV) is quite larger to that of ZnO (3.37 eV). However, oxygen vacancies are also responsible for band gap configuration in the samples. Band gap is a parameter which controls the photon absorption. Further the wide band gap of the doped compounds is appropriate for high temperature and high power processing with low electronic noise and also has the potential to sustain large electric fields.

The non-centro symmetric crystal structure with polar Zn–O bonds of wurtzite ZnO explores the ferro [27, 28], piezo and pyro electricity in the compound. Ferromagnetism has also been perceived in pristine ZnO at room temperature. The ferromagnetic nature of ZnO is ascribed to the appearance of carrier vacancies and interstitials in the sample [29]. The physical properties like electrical conductivity, dielectric, magnetic etc. of a semiconductor can easily be controlled by suitable doping. Ferromagnetic property has been noticed recently in non-magnetic element like lithium and magnesium doped ZnO [148-150].

The modification of optical, photocatalytic, magnetic and ferroelectric properties in doped ZnO compounds depend on its growth technique. In literature study, though we have come across some works on the photocatalytic and ferromagnetic nature of Mg-doped ZnO, very few articles have been found on dielectric behavior of Mg-modified ZnO [151]. Report on multiferroicity and ME coupling of ZnO materials is very rare. In literature study just a single report has been noticed on the sunlight-driven photocatalytic applications of Mg-doped ZnO nanoparticles [85]. Thus interest has been generated to investigate the optical, photocatalytic, multiferroic and ME coupling properties of Mg-doped ZnO nanoparticles. Here we report these studies on $Zn_{1-x}Mg_xO$ (x = 0, 0.03, 0.06, 0.09, 0.12, 0.15) nanoparticles synthesized through simple chemical precipitation method.

6.2. Experimental procedures:

6.2.1. Synthesis of pure and Mg-doped ZnO:

The $Zn_{1-x}Mg_xO$ (x = 0.00, 0.03, 0.06, 0.09, 0.12, 0.15) nanoparticles were synthesized through simple chemical precipitation method. Here, zinc acetate dihydrate, magnesium acetate [$Mg(CH_3COO)_2$, $4H_2O$] and sodium hydroxide (1.5 M) were taken as precursor materials and double distilled water was used as solvent. 0.5 M solutions of acetates were prepared through constant stirring using a magnetic stirrer. Initially the temperature of

acetate solution was raised to 70 ^{o}C by water heat bath. Then requisite amount of 1.5 M NaOH solution is mixed to the solution of acetates to grow up precipitates. The experimental temperature was retained at 70 ^{o}C to increase the reaction rate and is an accepted technique for the preparation of ZnO nanopowders. The precipitated nanopowders of $Zn_{1-x}Mg_xO$ were separated through centrifuge at 9500 rpm for 5 minutes for 5 times using ethanol and double distilled water as cleanse solvent. The precipitates were then dried at 120 ^{o}C and the dried nanopowders were calcined at 500 ^{o}C for 2 hour. After calcination the materials were compressed with isostatic press (7.9×10^5 N/m^2) for pellet shape and the prepared pellets were sintered at 600 ^{o}C for 3 hour.

6.2.2. Characterization techniques:

The Mg-doped ZnO nanoparticles were characterized by XRD, HRTEM, FTIR, UV-Vis absorption, FL, dielectric, ferroelectric, SQUID and ME coupling measurements as discussed in sec 2.2 of chapter 2.

Measurement of photocatalytic activity:

Photocatalytic performance of Mg-doped ZnO nanoparticles were determined by sunlight-irradiated degradation of methylene blue (MB). Here xenon lamp with 0.68 W/m^2 power was used as the source of light. First a solution of methylene blue was prepared by dissolving 50 mL of 1×10^{-5} M MB in double distilled water. Then a uniform dispersion of 0.08 gm Mg-doped ZnO nanopowder in 80 ml MB solution was prepared using ultrasonic vibrator. The prepared suspension was stirred in dark condition for 30 minute to reach adsorption equilibrium. Then the suspension was exposed to simulated sunlight (0.68 W/m^2) under constant stirring. The temperature of the suspension was sustained at 25 ^{o}C. After a particular time interval the aliquots were taken from the suspension and then centrifuged immediately. The degradation of MB was studied by using UV-Vis spectrophotometer

(Perkin-Elmer, Lamda 35). The photocatalytic rate constant (k) for MB degradation was calculated from the first-order kinetic eqn. $\ln\left(\frac{A_0}{A}\right) = kt$ (6.1)

where A_0 and A is the initial absorbance and absorbance after a particular time interval t respectively and k is the first-order kinetic rate constant. The schematic view of photocatalytic set-up is exhibited in figure 6.1.

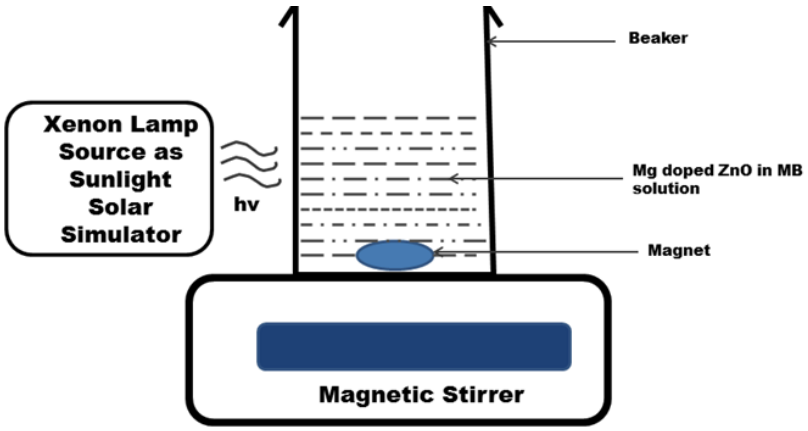

Fig. 6.1. Photocatalytic set-up for MB degradation by Mg-doped ZnO.

6.3. Result and discussions:

6.3.1. The kinetics of synthesis:

For synthesis of the compounds, zinc acetate dihydrate, magnesium acetate and sodium hydroxide (1.5 M) were taken such that the mole number of $(OH)^-$ ions in the solution is in the ratio of 1:3 to 1:4 with the number of moles of the Zn^{2+} and Mg^{2+} ions taken together. White colloidal solution of zinc hydroxide [$Zn(OH)_2$] and magnesium hydroxide [$Mg(OH)_2$] is formed as per the following chemical equations:

$$Zn(CH_3COO)_2, 2H_2O + 2NaOH \rightarrow Zn(OH)_2 + 2CH_3COONa + 2H_2O \quad (6.2)$$

$$Mg(CH_3COO)_2, 4H_2O + 2NaOH \rightarrow Mg(OH)_2 + 2CH_3COONa + 4H_2O \quad (6.3)$$

The experimental temperature was maintained at 70 ^oC and the solution was stirred continuously for 2 hours during which the $Zn(OH)_2$ and $Mg(OH)_2$ with excess hydroxyl ions transform to $[Zn(OH)_4]^{2-}$ and $[Mg(OH)_4]^{2-}$ respectively and are the nucleation centers of the

crystal. Concentrations of $(OH)^-$ ion in excess of the 1:4 ratio with metal ions is expected to form a capping layer inhibiting crystal growth. The reaction between $[Zn(OH)_4]^{2-}$ and $[Mg(OH)_4]^{2-}$ form $Zn_{1-x}Mg_xO$ nanopowders as per the equation:

$$(1-x)[Zn(OH)_4]^{2-} + x\,[Mg(OH)_4]^{2-} \rightarrow Zn_{1-x}Mg_xO + H_2O + 2(OH)^- \quad (6.4)$$

The precipitated nanopowders were separated through centrifuge using ethanol and double distilled water as cleanse solvent. It is worth mentioning here that while the standard enthalpy of creation of ZnO and MgO at 300 K is −350 kJ/mol and −601 kJ/mol, the standard values of entropy for these materials are 26.85 J/mol-K (0.28 meV/FU-K) and 43.65 J/mol-K (0.45 meV/FU-K) respectively. The formation enthalpy ΔH of $Zn_{1-x}Mg_xO$ nanoparticles with respect to separation into wurtzite ZnO crystal and rocksalt MgO is normally determined from the relation

$$\Delta H(Zn_{1-x}Mg_xO) = H(Zn_{1-x}Mg_xO) - [x\,H(MgO) + (1-x)\,H(ZnO)] \quad (6.5)$$

Where, H is the enthalpy of $Zn_{1-x}Mg_xO$ in hexagonal wurtzite phase and MgO in cubic rocksalt phase. The formation energy of $Zn_{1-x}Mg_xO$ nanoparticles is indicated to reveal a linear variation with x for $x \leq 0.2$ [271-273]. The reported formation energy of $Zn_{1-x}Mg_xO$ in the hexagonal wurtzite structure per formula unit, with the miscibility is around $3.54*x$ meV/FU for a concentration of x% of doped Mg. For prepared $Zn_{1-x}Mg_xO$ samples with x = 0.03-0.15 the formation energy lies within 10.62 meV/FU (1.02 kJ/mol) to 53.1 meV/FU (5.1 kJ/mol) [273]. As such the reaction can proceed at room temperature wherein the thermal energy is equal to 39 meV [274]. However, the reaction temperature is maintained at 70 ^oC to increase the reaction rate. The smaller values of formation energy denote stability of $Zn_{1-x}Mg_xO$ nanoparticles without getting dissociated into the binary compounds ZnO and MgO [271]. The smaller ionic radius of Mg^{2+} ions compared to that of Zn^{2+} ions ensures somewhat relaxation in the structure. However, with increase in concentration of Mg,

structural instability sets in $Zn_{1-x}Mg_xO$ nanoparticles owing to structural inconsistency between ZnO and MgO. The mixing entropy of $Zn_{1-x}Mg_xO$ materials with x in the range 0.03 and 0.15 from the binary compounds ZnO and MgO remain in the range of 0.01 meV/FU-K (1 J/mol-K) to 0.035 meV/FU-K (3.37 J/mol-K) [275].

6.3.2. XRD analyses:

The XRD data has been analyzed to investigate the crystal structure of the nanoparticles. The X-ray diffraction pattern of Mg-doped ZnO nanopowders are exhibited in figure 6.2. Peaks at same Bragg angle are explored by all $Zn_{1-x}Mg_xO$ (x = 0, 0.03, 0.06, 0.09, 0.12, 0.15) samples. The XRD analysis endorses that all the prepared samples with different mole percentage of Mg possess the crystal structure of hexagonal wurtzite with space group $P6_3mc$. The diffraction peaks obtained at 2θ = 31.82°, 34.34°, 36.30°, 47.55°, 56.63° and 62.83° correspond to (100), (002), (101), (102), (110) and (103) planes respectively have been verified with the available JCPDS file No. 36-1451 of ZnO [276]. Thus the XRD data approve the proper replacement of Mg ions at the Zn sites of host ZnO and also confirm that the solubility limit of Mg in wurtzite ZnO is well beyond 15 mole percentage. The average crystallite size (D) of the materials can be obtained from the Scherrer formula $D = \frac{k\lambda}{\beta Cos\theta}$ [277] as stated earlier. The crystallite size of the nanoparticles for diffraction peaks from planes (100), (002) and (101) have been determined and presented in table-VII. The crystallite diameters of doped ZnO (34-36 nm) are smaller than that of pure ZnO nanoparticles. The doped Mg^{2+} ion in host ZnO restrain the crystal growth because of smaller radius of Mg^{2+} ion than that of Zn^{2+} ion [278]. The lattice parameters have been calculated by POWDMULT software and displayed in table-VIII. The lattice parameters values of pure and doped ZnO are comparable with the standard informed values of $a = b$ = 3.248 Å, and c = 5.205 Å [253]. The c/a ratios for all the prepared samples remain near to

the actual value of 1.633 and are displayed in table-VIII. The Zn–O bond lengths of the nanoparticles are calculated using the formula $L=\sqrt{\frac{a^2}{3}+\left(\frac{1}{2}-u\right)^2 c^2}$, where $u=\frac{a^2}{3c^2}+0.25$ [227] and also provided in the table-VIII. Although, in the doped compounds Mg^{2+} ions substitute at the Zn^{2+} sites of host ZnO, the average bond length decreases because in reality the Mg–O bond length is shorter by nearly 0.23Å than Zn–O bond length.

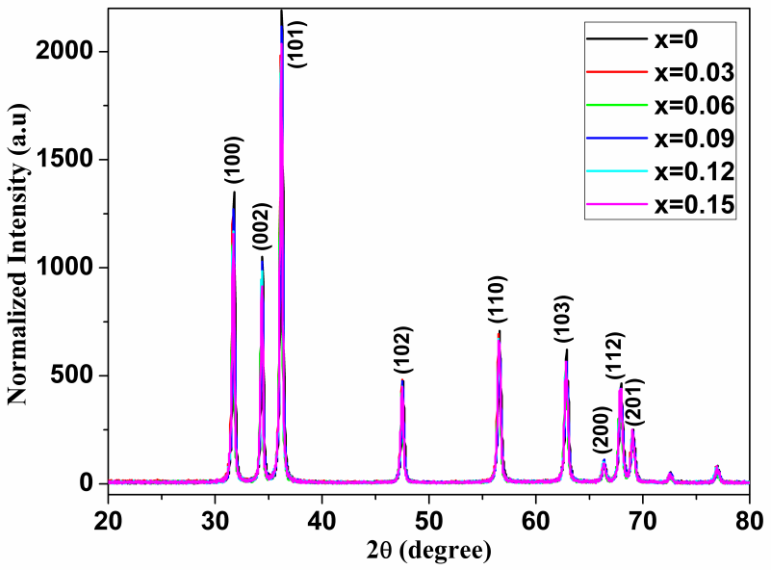

Fig. 6.2. XRD patterns of $Zn_{1-x}Mg_xO$ samples.

Table-VII. The average crystallite diameter of $Zn_{1-x}Mg_xO$ series.

Sample	D (nm) from (100) peak	D (nm) from (002) peak	D (nm) from (101) peak	Average D (nm)
ZnO	34.97	39.44	34.98	36.46
$Zn_{0.97}Mg_{0.03}O$	33.58	38.50	34.57	35.55
$Zn_{0.94}Mg_{0.06}O$	34.47	37.02	34.16	35.22
$Zn_{0.91}Mg_{0.09}O$	33.35	39.01	33.31	35.22
$Zn_{0.88}Mg_{0.12}O$	34.88	37.99	34.00	35.62
$Zn_{0.85}Mg_{0.15}O$	32.52	33.67	34.17	33.45

Table-VIII. Lattice parameter a and c value of Mg-doped ZnO nanoparticles.

Sample	a in Å	c in Å	c/a	Zn–O bond length (Å)
ZnO	3.257	5.207	1.598	1.774348
$Zn_{0.97}Mg_{0.03}O$	3.254	5.209	1.60	1.771804
$Zn_{0.94}Mg_{0.06}O$	3.254	5.211	1.601	1.771536
$Zn_{0.91}Mg_{0.09}O$	3.250	5.204	1.601	1.769438
$Zn_{0.88}Mg_{0.12}O$	3.250	5.207	1.602	1.769036
$Zn_{0.85}Mg_{0.15}O$	3.249	5.202	1.601	1.768947

6.3.3. HRTEM and SAED:

The internal morphology, crystallinity and elemental composition of doped ZnO nanopowders have been analyzed by HRTEM, SAED and EDX. The TEM micrographs of 6%, 12% and 15% Mg-modified ZnO nanoparticles are presented in figure 6.3(a), 6.3(b) & 6.3(c) and the HRTEM image of 15% Mg-doped ZnO nanostructures is displayed in figure 6.4. The TEM photograph exhibits nearly spherical shape of the Mg-doped ZnO nanocompounds having average particle size of 25 nm. The interplanar spacing of the 15% Mg-doped sample is found to be 0.28 nm from the HRTEM photograph. The interplanar spacing d_{hkl} for the hexagonal wurtzite structure is determined according to the relation [255]

$$d_{hkl} = \left[\frac{4}{3}\left(\frac{h^2 + hk + k^2}{a^2} \right) + \frac{l^2}{c^2} \right]^{-\frac{1}{2}}.$$

Using the lattice parameters from table-VIII, the calculated value of d_{100} for $Zn_{0.85}Mg_{0.15}O$ amounts to 0.281 nm and is in well agreement with the HRTEM capture. Thus the growth direction of the specimen considering for HRTEM is [100] direction and is in agreement with the earlier reported findings [194]. The distributions and different direction of orientations of the grains have been observed from the TEM photographs for various doped nanoparticles. The SAED pattern for $Zn_{1-x}Mg_xO$ nanopowders with x = 0.12 and 0.15 are displayed in figure 6.5(a) and 6.5(b) respectively. The crystalline nature and the hexagonal shape of the samples are explored by the SAED photographs. The SAED pattern clearly exhibits the bright rings and spotty dots as presented in figure 6.5(b) attribute to the diffraction peaks of (100), (002), (101) etc. of the hexagonal wurtzite structure similar to earlier literature [279]. This pattern gets evolved due to the polycrystalline nature of the nanopowder. However, the SAED pattern of figure 6.5(a) for the sample with x = 0.12 displays bright spotty dots originated due to single crystalline nanoparticle. Here, it is worth informing that the particle size calculated from XRD study and TEM analysis have same values mentioning a mono particle grain.

The EDX spectrum of 15% Mg-doped ZnO nanoparticles are displayed in figure 6.6 which confirms the elements Mg, Zn and O are present in the compound. The Cu peaks of EDX spectrum are originated from the carbon coated copper grid used for the TEM analysis.

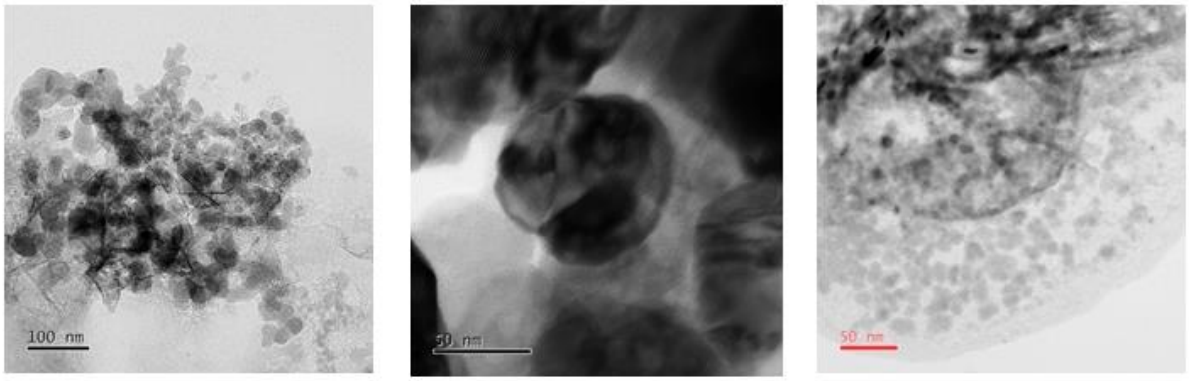

(a) **(b)** **(c)**

Fig. 6.3. TEM image of **(a)** $Zn_{0.94}Mg_{0.06}O$, **(b)** $Zn_{0.88}Mg_{0.12}O$ and **(c)** $Zn_{0.85}Mg_{0.15}O$ samples.

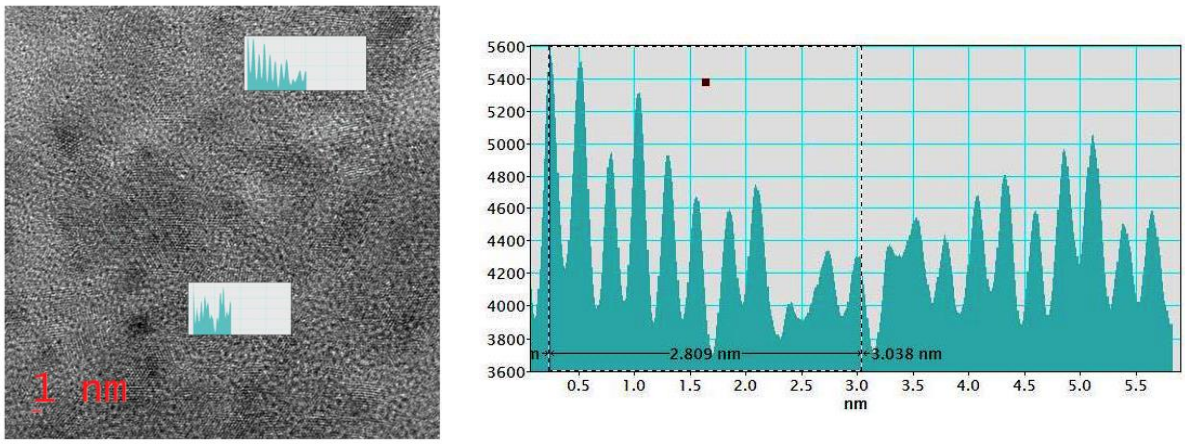

Fig. 6.4. HRTEM image of $Zn_{0.85}Mg_{0.15}O$ sample.

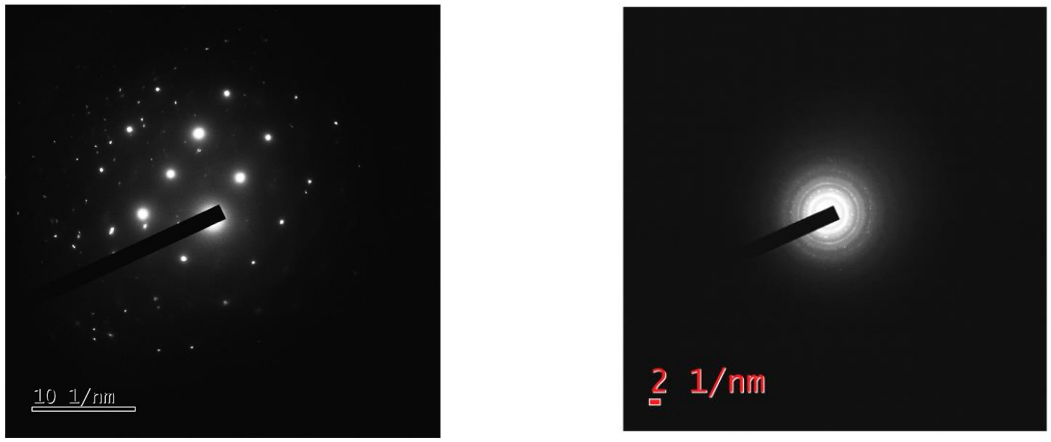

(a) **(b)**

Fig. 6.5. SAED patterns of **(a)** $Zn_{0.88}Mg_{0.12}O$ and **(b)** $Zn_{0.85}Mg_{0.15}O$ samples.

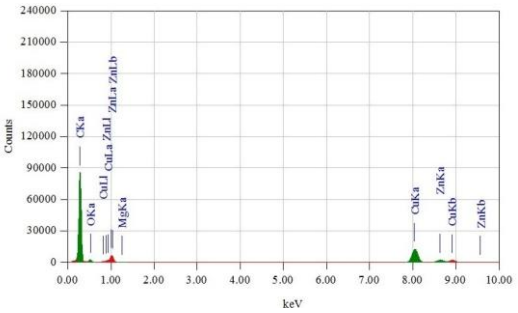

ZAF Method Standardless Quantitative Analysis
Fitting Coefficient : 0.0852

Element	(keV)	Mass%
C K	0.277	93.18
O K*	0.525	2.46
Mg K*	1.253	0.01
Cu K	8.040	4.31
Zn K	8.630	0.05
Total		100.00

Fig. 6.6. EDX pattern of $Zn_{0.85}Mg_{0.15}O$ sample.

6.3.4. FTIR:

The FTIR spectra of Mg-doped ZnO samples have been investigated between the wave number regions of 400-4000 cm^{-1} and are presented in figure 6.7. The wide transmission bands of 3444 cm^{-1} are ascribed to stretching vibrations of hydroxyl (OH) group of water in the nanopowder sample [280, 281]. The peak 2343 cm^{-1} corresponds to CO_2 present in the samples for measurement of FTIR [247, 203]. The peaks identified at 1398 cm^{-1} are accredited to COO^- symmetric stretching vibration [205]. One large band perceived at 450 to 530 cm^{-1} belongs to Zn–O stretching of hexagonal wurtzite ZnO structure [10, 195]. In case of Mg-doped nanosamples the band is slightly shifted towards lower wave numbers. In fact the absorption band of Mg–O stretching vibration is conveyed between 450-510 nm and overlaps with that of Zn–O [282]. The identical nature of FTIR spectra for all the nanoparticles endorses the Mg incorporation in host ZnO.

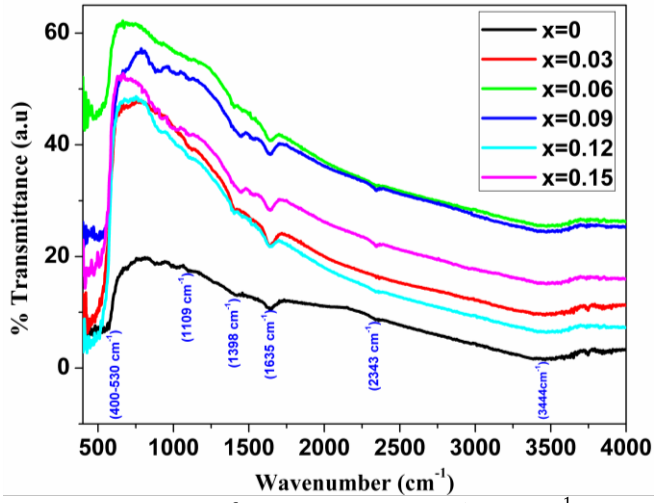

Fig. 6.7. FTIR spectra of $Zn_{1-x}Mg_xO$ series (400 cm^{-1} - 4000 cm^{-1}).

6.3.5. UV-Vis spectroscopy:

The absorption spectra of $Zn_{1-x}Mg_xO$ nanoparticles with various Mg doping concentrations have been investigated in the wavelength region of 300-800 nm and are displayed in figure 6.8(a). The absorption peaks have been found at 381, 375, 378, 378, 379, 381 nm for different Mg concentrations of x = 0, 0.03, 0.06, 0.09, 0.12, 0.15 respectively. These peaks are ascribed to large excitons with fundamental absorption [10, 220]. The energy gap has been assessed from the point of inflection which relates to the maxima, obtained through the first order differentiation of Gaussian fitting to the respective energy of absorbance. The calculated energy band gap amounts to 3.261 eV, 3.304 eV, 3.278 eV, 3.269 eV, 3.265 eV and 3.268 eV respectively for x = 0, 0.03, 0.06, 0.09, 0.12, 0.15. The perceived band gap of all the ZnMgO nanoparticles is little higher than that of ZnO. The highest band gap is obtained for the sample with x = 0.03 and the band gap appears to decrease a bit with further increase in Mg concentration. This feature is verified in the current density vs. electric field graph shown as figure 6.8(b) wherein the sample with x = 0.03 have the lowest conductivity and the conductivity increases with increasing Mg concentration preserving an inverse relation with band gap.

With the doping of Mg in host ZnO, the energy band gap is expected to increase as because the energy gap of MgO (7.4 eV) is much higher to that of ZnO (3.4 eV). In such a situation the addition of Mg in ZnO is predicted to increase the band gap which is quite larger than what is perceived. The difference in the perceived band gap can be entrusted to the reduction of oxygen vacancy in the nanoparticles. ZnO crystals prepared through various techniques are almost always *n*-type [283]. The reason of *n*-type formation in ZnO is under controversy till now. Yet it is assumed that oxygen vacancy (V_O) is a common indigenous point defect that creates higher density of electron close to the band edge and moves the Fermi level towards the conduction band as explained in Moss-Burstein effect [208, 209].

The energy band gap is the value of excitation energy of an electron from top of the valence band into an energy level above the Fermi level.

According to the difference of electronegativity Mg–O bond is more ionic as the tune of 2.13 between Mg and O than that of 1.79 in ZnO. The Mg–O bond is shorter and stronger than that of Zn–O with an amount of 0.23Å that suppresses some oxygen vacancies. Consequently, a decrement in the *n*-type character and a lowering in the position of Fermi level decrease the band gap. These two contending effects decide the optical band gap in the ZnMgO nanoparticles. Under such a condition a small increase in the apparent band gap is achieved in these compounds than that of host ZnO.

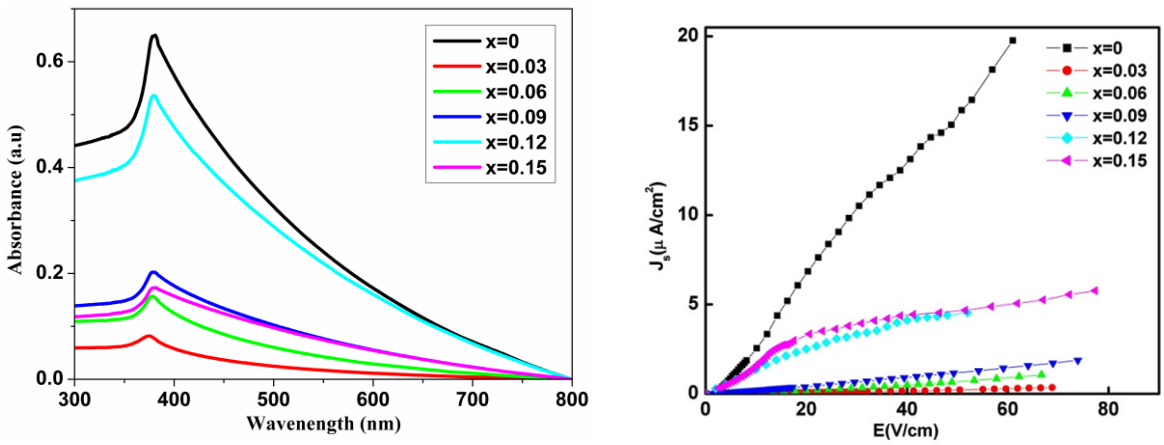

Fig. 6.8. **(a)** Absorption spectra of $Zn_{1-x}Mg_xO$ series and **(b)** Current density vs. electric field graph.

6.3.6. Fluorescence:

The fluorescence spectra of pure and Mg-modified ZnO nanoparticles at room temperature with the excitation of 325 nm are presented in figure 6.9. Two emission peaks at 360 and 382 nm in the ultraviolet (UV) region and a peak at 468 nm of blue region are observed in the FL spectra for all Mg-doped and pure ZnO nanoparticles. The strong UV emission peaks relating to near-band-edge emission are created due to the radiative recombination of electron (e_{CB}^-) and hole (h_{VB}^+) in the conduction and valence band respectively [284]. The emission peak at 382 nm of pure ZnO is shifted towards lower

wavelength for Mg-modified ZnO. This denotes that the band gap energy of Mg-doped ZnO is higher than pure ZnO nanoparticles. The shift in the FL spectra confirms our UV-Vis absorption findings regarding the band gap energy being highest in the compound with x = 0.03 and decrease a bit with further increase in doping concentration. The weak emission peak at 468 nm in the blue region has defect mediated origin [220]. Generally in ZnO nanocompounds interstitial zinc (Zn_i) and oxygen vacancy (V_O) act as donors, while interstitial oxygen (O_i) and zinc vacancy (V_{Zn}) as acceptors. Between above point defects, only Zn_i acts as a shallow donor and the reliable defect level have located below the conduction band-edge. The blue emission is the consequence of transition from the shallow donor level to the valence band [285].

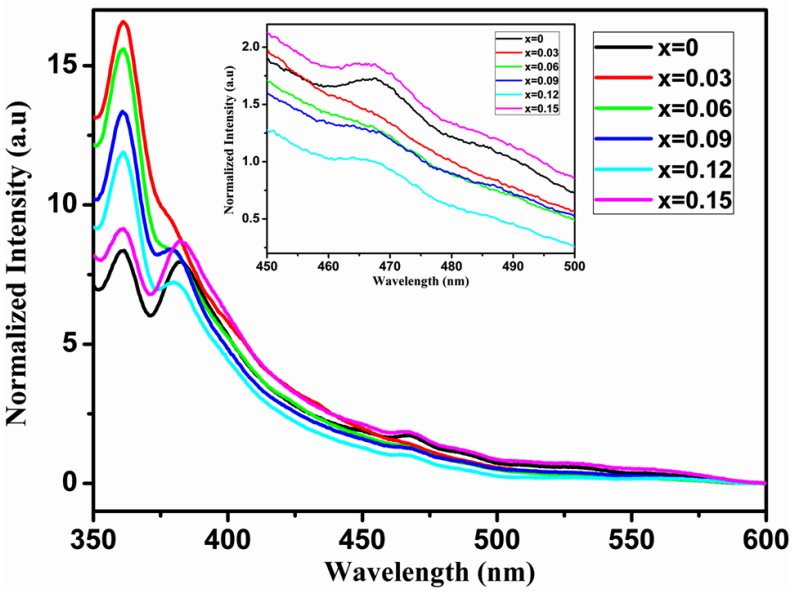

Fig. 6.9. FL spectra of $Zn_{1-x}Mg_xO$ series.

6.3.7. Photocatalytic activity:

Photocatalytic degradation of MB under sunlight irradiation by Mg-doped ZnO nanoparticles are exhibited in figure 6.10(a-f). Mg-doped ZnO samples conduct photocatalytic activity with the photocatalysis performance increasing with increase in the doping concentration as depicted in figure 6.11. Photocatalytic reactions are fashioned by $OH^{\bullet}$ and $O_2^{\bullet-}$ radicals twisted on surface of the Mg-doped ZnO samples [88].

$$ZnMgO + h\nu \rightarrow e_{cB}^{-} + h_{vB}^{+} \quad (6.6)$$

$$H_2O + h_{vB}^{+} \rightarrow OH^{\bullet} + H^{+} \quad (6.7)$$

$$O_{2(ads)} + e_{CB}^{-} \rightarrow O_2^{\bullet -} \quad (6.8)$$

$$OH_{(ads)}^{-} + h_{vB}^{+} \rightarrow OH_{(ads)}^{\bullet} \quad (6.9)$$

The photocatalytic rate constants for pure ZnO and 3%, 6%, 9%, 12% and 15% Mg-doped ZnO are found to be 0.013, 0.015, 0.02, 0.028, 0.038, 0.052 min^{-1} respectively [286]. The higher redox potential of the photo-generated electron-hole pairs results from higher band gap energy, which significantly enriches the photocatalytic activity [85]. In consequence, Mg-doped ZnO nanoparticle provides better photocatalytic activity comparing with pure one. The photocatalytic activity of 3% Mg doping is lower though the sample possesses highest band gap energy as compared to other compositions of Mg-doped ZnO nanoparticles. This aspect is most possibly due to its greater crystallite size and consequent lower surface area per mole than other Mg-doped ZnO nanocompounds.

Mg-doped ZnO realizes better MB degradation performance rather pure ZnO due to alterations of chemical and physical properties of ZnO. Here the recombination of photo-generated electron-hole pairs is inhibited by smaller crystallite size of doped ZnO and therefore the photocatalytic activity is enhanced. Mg incorporation in host ZnO could produce more surface defects and in result a space charge layer could be made on the surface enabling the migration of photo-induced charge carriers toward surface defects [287]. Hence the separation efficiency of electron-hole pairs in Mg-modified ZnO nanocompounds becomes greater than the pure ZnO and an improvement in photocatalytic performance proceeds with increasing Mg concentration. Therefore, the superior photocatalytic performance of doped ZnO nanoparticles accredited to the surface defects and crystallite size which are established earlier by FL spectra and XRD analyses respectively. Hence in

conclusion it is conveyed that the photocatalytic performance of these Mg-doped ZnO nanocompounds is being organized by the three contending factors: band gap, crystallite size and surface defect.

Intensity of fluorescence spectra and photocatalytic activity are strongly interrelated with each other because the FL emission arises from the recombination of photo-generated charge carriers [288-290]. Reduced near band edge (NBE) and excitonic emission peak intensities specified for the most active 15% Mg-doped ZnO nanoparticles as compared to other Mg-modified ZnO samples results in better photocatalytic effect. Further, relatively small photo-active $Zn_{0.97}Mg_{0.03}O$ has explored highest fluorescence emissions which exhibit faster recombination of electron-hole pairs. Both the emission intensity and photocatalytic activity of undoped ZnO are small compared to all the Mg-doped ZnO nanosamples because of its moderately small band gap and bigger crystallite size.

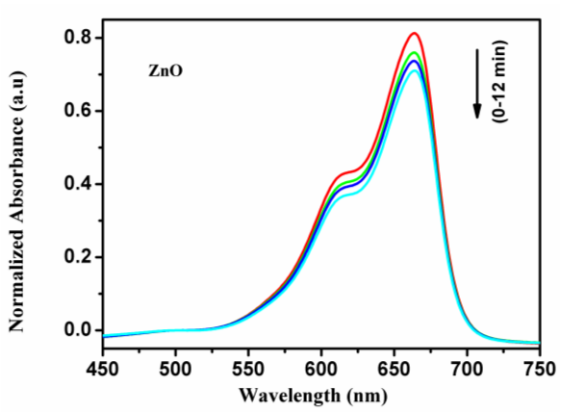

(a)

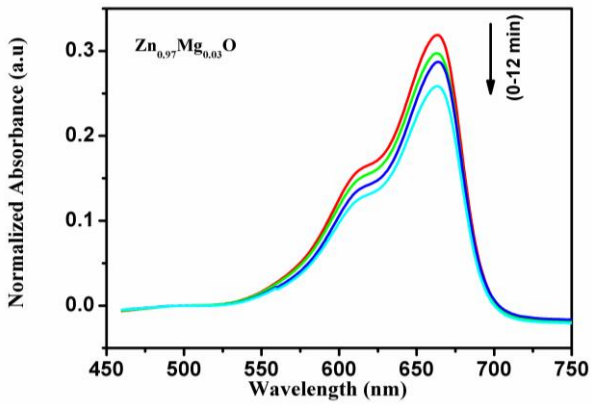

(b)

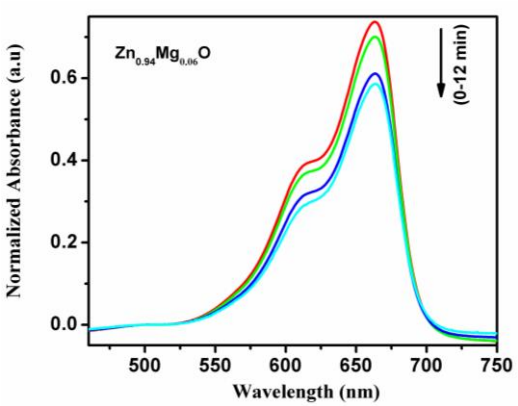

(c)

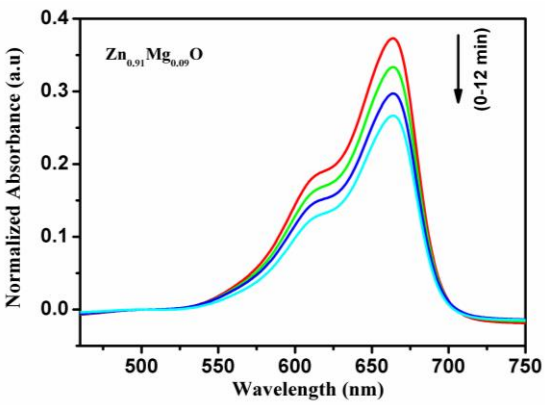

(d)

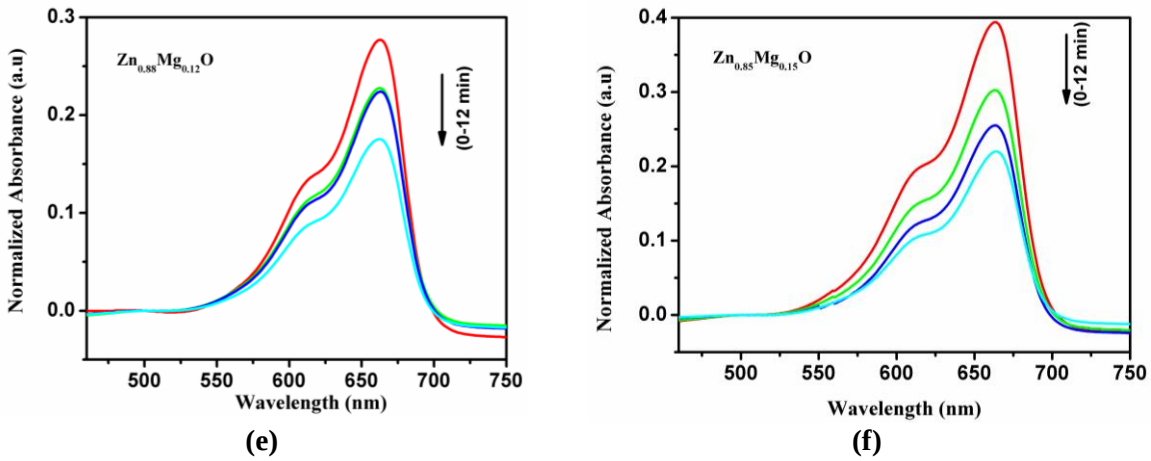

Fig. 6.10. Photocatalytic degradation of **(a)** pure ZnO, **(b)** $Zn_{0.97}Mg_{0.03}O$, **(c)** $Zn_{0.94}Mg_{0.06}O$, **(d)** $Zn_{0.91}Mg_{0.09}O$, **(e)** $Zn_{0.88}Mg_{0.12}O$ and **(f)** $Zn_{0.85}Mg_{0.15}O$.

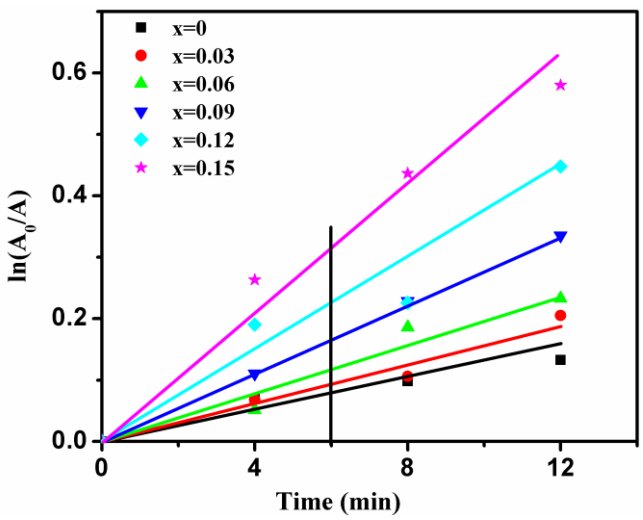

Fig. 6.11. Kinetic study of MB degradation by $Zn_{1-x}Mg_xO$.

6.3.8. Dielectric property:

The variation of dielectric constant (έ) and dielectric loss (tanδ) of the nanoparticles at room temperature have been investigated in the frequency range of 100 Hz-100 kHz and are presented in figure 6.12(a) and 6.12(b). The usual decreasing tendency of total polarization with increasing frequency, originating from dipoles and trapped charge carriers, is maintained by all Mg-doped ZnO nanoparticles. In these compounds, at low frequency the existence of oxygen vacancies, grain boundary defects etc. [151] subscribe to very high dielectric constant and can be analyzed by Maxwell–Wagner interfacial model [233, 291] and Koop's

phenomenological theory [292]. Further a decreasing nature is observed in dielectric constant (έ) and loss tangent (tanδ) with Mg concentration in the host ZnO for the entire frequency region. This is because of the decrease of oxygen vacancy. Decrease of oxygen vacancy means decrease in *n*-type character which in result decreases the dielectric constant and also the loss tangent. With decrease in *n*-type character, the conducting loss which is dominant at low frequencies also decreases causing a decrease in loss tangent. Dielectric constant and the loss tangent of all samples become almost constant at higher frequencies because the electron exchange between dopant ions and host matrix is unable to follow an alternating field.

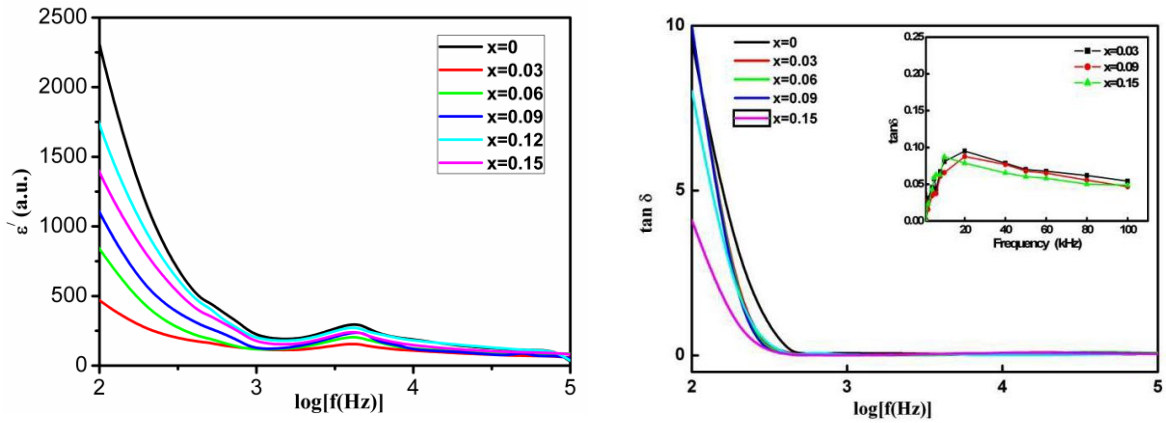

Fig. 6.12. Variation of **(a)** έ and **(b)** tanδ with frequency and composition of $Zn_{1-x}Mg_xO$.

However, an anomaly at 6 kHz is observed in dielectric constant while a relaxation peak is exhibited at around 20 kHz in the loss tangent, as displayed in the inset figure.

6.3.9. P-E analyses:

The Mg-modified ZnO nanocompounds exhibit ferroelectric nature at room temperature as displayed in figure 6.13. Small remnant polarization with small coercive field has been observed from slim hysteresis loops for these compounds. The remnant polarization of the $Zn_{0.91}Mg_{0.09}O$ and $Zn_{0.85}Mg_{0.15}O$ nanosamples are found to be 0.076 and 0.054 $\mu C/cm^2$ [293].

The polarization varies with frequency, depending on dipolar and space charge polarization. Dipole moment is the measure of dipolar polarization which ultimately determined by the bond length of the ZnO and MgO compounds. The relation between polarization and square of the dipole moment is proportional at low field. The length of Zn–O bond is about 1.978Å and that of Mg–O is 1.743Å. The shorter bond length of Mg–O is expected to decrease the remnant polarization as the number of Mg–O bonds increases in compounds with higher Mg doping concentration in ZnO matrix. Few works also recommend that the smaller Mg^{2+} ion without *d* electrons in ZnO matrix will progress the ionic character and squeeze the Zn–O bond along the polar *c*-axis [294, 295]. Consequently a small structural distortion might be created which causes a decrease in remnant polarization [266].

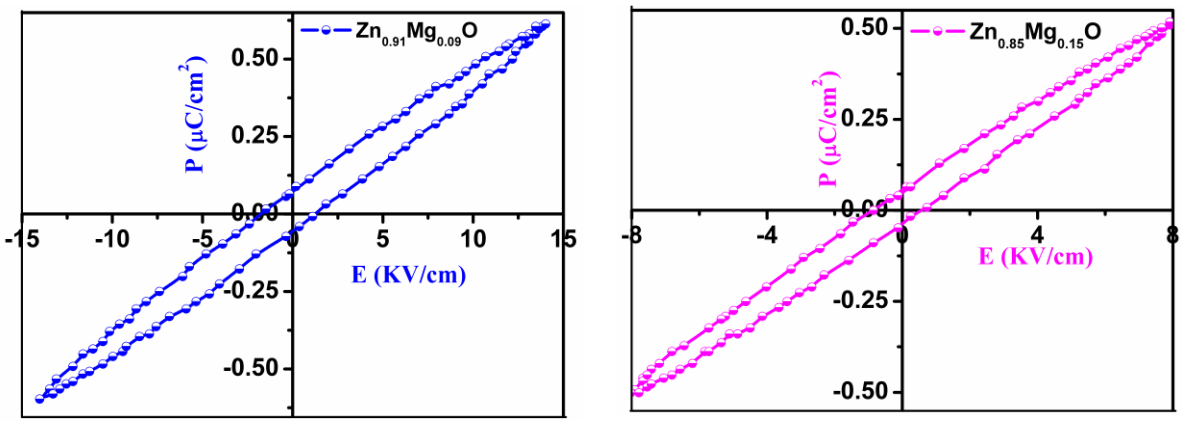

Fig. 6.13. P-E loop of $Zn_{0.91}Mg_{0.09}O$ & $Zn_{0.85}Mg_{0.15}O$ samples.

6.3.10. Magnetic property:

The magnetic property of $Zn_{0.85}Mg_{0.15}O$ sample has been carried out with applied field of ±1 T at 5K by using SQUID. Figure 6.14 represents hysteresis curve for the sample at experimental temperature indicating ferromagnetic behavior in the sample. The magnetism in a sample can be assigned too many reasons i.e. extrinsic causes (impurity clusters, extra phases, or contaminants) or intrinsic causes (exchange interactions between carriers and local moments). In our study, XRD and EDX analyses confirms the absence of any extra phase or

contaminant. So here ferromagnetism arises may be due to intrinsic exchange interaction. Ferromagnetism in metal oxide nanoparticles, like CeO_2, Al_2O_3 and ZnO etc. have been assigned by many research groups to the interaction between localized spin moments generated by the oxygen vacancies [238]. The presences of oxygen vacancies have been confirmed in the UV–Vis absorption and dielectric analysis. A plausible explanation for the observed magnetic behavior in the sample may be based on the concept that the inherent oxygen vacancies present in the host ZnO matrix trap the charge carriers resulting in the formation of bound magnetic polarons. The interaction between these bound magnetic polarons is most likely the cause behind the ferromagnetic behavior of Mg-doped ZnO samples.

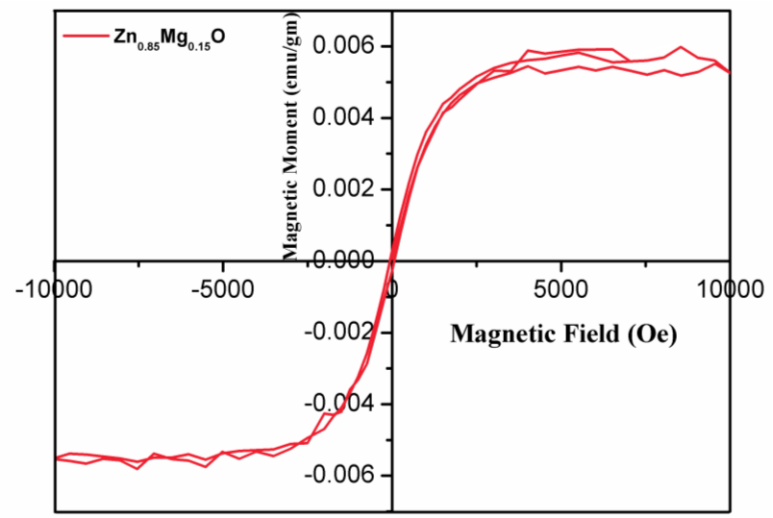

Fig. 6.14. M-H loop of $Zn_{0.85}Mg_{0.15}O$ sample.

6.3.11. ME analyses:

The occurrence of multiferroic natures in the compounds advances the possibility for electromagnetic coupling in the nanoparticles. Though the magnetic properties have been studied in literature, we have not come across any report on the ME coupling of the compound. The ME voltage coupling coefficient at room temperature for the compounds $Zn_{0.91}Mg_{0.09}O$ and $Zn_{0.88}Mg_{0.12}O$ is exhibited in figure 6.15(a) and 6.15(b). The sample was exposed to electrical and magnetic poling as stated in sec. 2.2.8 before set for ME

measurements. The ME voltage coefficient (α_E) [188, 189] for the two samples $Zn_{0.91}Mg_{0.09}O$ and $Zn_{0.88}Mg_{0.12}O$ amounts to 3.150 and 4.131 mV/(cm Oe) respectively. These values are moderately significant comparing with many other compounds. The ME coupling becomes stronger with increasing Mg percentage in host ZnO. The second order coefficients (β) and third order coefficients (γ) for the $Zn_{0.91}Mg_{0.09}O$ sample have values -1.93×10^{-6} mV/(cmOe^2) and 8.37×10^{-11} mV/(cmOe^3) respectively. The corresponding values for $Zn_{0.88}Mg_{0.12}O$ amounts to -2.75×10^{-6} mV/(cmOe^2) and 3.737×10^{-12} mV/(cmOe^3). So the linear term is extremely prominent term and highly advantageous for applications in any device.

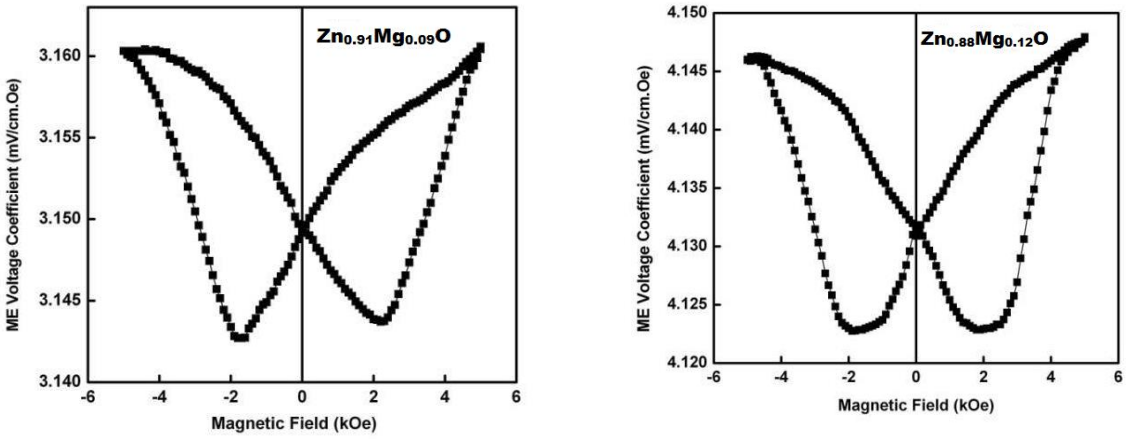

(a) **(b)**

Fig. 6.15. ME loop of **(a)** $Zn_{0.91}Mg_{0.09}O$ and **(b)** $Zn_{0.88}Mg_{0.12}O$ samples.

6.4. Conclusions:

The pure and Mg-modified ZnO nanocompounds with superior physical and chemical properties have been prepared effectively through low-cost chemical precipitation method. XRD characterization confirms the successful replacement of Mg^{2+} at the Zn^{2+} sites of hexagonal wurtzite ZnO. The average crystallite grain size of the nanoparticles, determined from XRD is 34 nm and that from TEM characterization is 25 nm. Single crystallinity is preserved in case of undoped and doped ZnO nanoparticles. The favored growth plane of the specimen, as captured in HRTEM, is along the (100) plane. Enhanced photocatalytic

performance has been achieved in Mg-doped ZnO nanoparticles. 15% Mg doping in the host ZnO enhances the photocatalytic rate constant of the ZnO by 300%. The superior optical and photocatalytic properties of Mg-doped ZnO nanoparticles suggest that it might be exploited for an efficient sunlight driven photocatalytic effect, self-cleaning and photovoltaic applications. The dielectric constant gives very high value at low frequency and maintains a constant value at high frequency. The decrease in the loss tangent in the Mg-doped samples, make them suitable for better dielectric applications. The doped ZnO nanocompounds have shown both ferroelectric and ferromagnetic characteristics and have the potentiality for applications in multiferroic devices. The ME coefficient of the prepared nanoparticles is significant and almost linear. This coefficient increases with increasing Mg concentration in host ZnO. Therefore the samples are also useful for the application in magnetoelectric coupling devices.

[Results of this work have been published in (i) Physica E: Low-dimen. Sys. Nanostruc. 104 (2018) 254-260 & (ii) Mater. Sci. Eng. B, 245 (2019) 1-8. (Ref. 286 & 293)]